Available online at www.sciencedirect.com

ScienceDirect

Proceedings of the Combustion Institute 37 (2019) 2335–2343

Proceedings of the Combustion Institute

www.elsevier.com/locate/proci

# Morphology of wrinkles along the surface of turbulent Bunsen flames – Their amplification and advection due to the Darrieus–Landau instability

Meng Zhang [a,b,*], Advitya Patyal [b], Zuohua Huang [a], Moshe Matalon [b]

[a] *State Key Laboratory of Multiphase Flow in Power Engineering, Xi'an Jiaotong University, Xi'an 710049, China*
[b] *Department of Mechanical Science and Engineering, University of Illinois at Urbana-Champaign, Urbana, IL 61801, USA*

Received 1 December 2017; accepted 26 June 2018
Available online 11 July 2018

**Abstract**

The morphological development of wrinkles along the surface of a Bunsen flame in a weakly-turbulent flow is investigated, with turbulence added solely to disturb the flame front. The resulting flame-flow interactions are examined using a hybrid Navier–Stokes/front-tracking methodology within the context of the hydrodynamic theory. Topological markers based on the skewness of curvature are introduced to distinguish between sub- and super-critical conditions, or the absence/presence of the Darrieus–Landau instability, respectively. We show that for sub-critical conditions disturbances created along the flame surface are dampened when convected downstream along the flame front, and the flame surface is only weakly perturbed. For super-critical conditions, on the other hand, disturbances of the flame front are amplified when advected downstream leading to a highly corrugated surface and a flame brush of increasing thickness. A measure of these dramatic changes is included in the mean local stretch rate which, when properly modulated by a Markstein length, directly affects the turbulent flame speed.


*Keywords:* Darrieus–Landau instability; Turbulent premixed flames; Bunsen flames; Markstein length; Inclined flames

## 1. Introduction

Studies of turbulent flames have often been carried out using a "planar configuration" where the flame propagates in one direction with periodic boundary conditions in all others. The flame in such a configuration can be considered as a segment of a much larger *freely propagating* flame. The growth/decay of perturbations on the surface of a planar flame depends primarily on the local flow conditions. In contrast, perturbations on the surface of laboratory flames, such as Bunsen, counterflow and spherically expanding flames, exhibit in addition, spatial and/or temporal variations initiated at their inception. For example, disturbances created near the burner rim of a Bunsen flame are advected downstream along the inclined

* Corresponding author at: State Key Laboratory of Multiphase Flow in Power Engineering, Xi'an Jiaotong University, Xi'an 710049, China.
*E-mail addresses:* mengz8851@xjtu.edu.cn, zhangmeng.hi@163.com (M. Zhang).

https://doi.org/10.1016/j.proci.2018.06.204
1540-7489 

flame front by the velocity component tangential to the flame surface and may grow in the presence of instabilities into spatially developing corrugations. The local flame conformation is therefore strongly influenced by the onset of the disturbances upstream and by their growth/decay. This would be particularly observed in tall flames that result at high flow rates, because the slanted section of the flame and hence, the mean velocity component tangential to the flame surface, are relatively large [1]. Driscoll [2] refers to this phenomenon as a "memory effect" and suggests that overall combustion properties, such as the turbulent flame speed, would depend in addition to turbulence and mixture properties on geometry-dependent parameters.

A key quantity characterizing premixed combustion is the turbulent flame speed $S_T$, defined as the mean propagation speed of a premixed flame into a turbulent mixture. Using a planar configuration, Damköhler [3] proposed that in the *large-scale turbulence regime* the ratio of the turbulent to the laminar flame speeds, $S_T/S_L$, is equal to the area ratio $\overline{A_f}/A$, where $\overline{A_f}$ is the mean surface area of the turbulent flame (over-bar representing an appropriately defined average) and $A$ is the surface area of the nominal planar flame. His argument was based on the assumption that (i) the mixture is locally consumed at a rate $\rho_u S_L$ where $\rho_u$ is the density of the fresh mixture and (ii) in the absence of turbulence, the planar flame is *stable*. Further advances in flame theory revealed that the local consumption rate of wrinkled flames is not constant; the local flame speed is given by

$$S_f = S_L - \mathcal{L}\mathbb{K} \tag{1}$$

where $\mathbb{K}$ is the stretch rate and $\mathcal{L}$ is the Markstein length [4,5]. Damköhler's argument revisited then yields

$$S_T/S_L = \overline{A_f S_f}/A S_L\,. \tag{2}$$

Moreover, the planar flame for $\mathcal{L}>0$ is, in general, unstable due to the Darrieus–Landau (DL) instability, unless its transverse dimension is sufficiently small and the stabilizing influences of diffusion dominate over the destabilizing effects of thermal expansion. In such circumstances, the turbulent flame speed in (2) must be compared to the speed $U_L$ of the *stable* cusped-like structure that results from the DL instability and not to the nominal planar flame which, in the absence of turbulence, is unrealizable. Since for weak turbulence intensities, $\overline{A_f S_f} \approx \overline{A}_f\,\overline{S}_f$, as suggested by the numerical simulations reported in [6], Eq. (2) can be replaced by

$$S_T/U_L \sim \left(1 - \mathcal{M}\overline{\mathbb{K}}\right)\left(\overline{A_f/A}\right) \tag{3}$$

where $\mathcal{M} = \mathcal{L}/L$ is the Markstein number, with $L$ an appropriately selected length scale characterizing the hydrodynamic field. As shown below, the mean stretch rate $\overline{\mathbb{K}}$ implicitly accounts for the geometry-dependence alluded to by Driscoll [2], because the local stretch rate is not constant but varies along the flame surface. Earlier attempts to capture the amplification of perturbations due to the DL instability on inclined flames and the dependence on their spatial inception, have been carried out by Boyer and Quinard [7] and Searby et al. [1] on Bunsen and V-flames. They observed that the transition from absolute (temporal) to convective instability occurs for a finite flow velocity, when the ratio of the tangential component of the flow velocity relative to the flame speed is sufficiently large. Support for this finding was provided by stability consideration based on the Michelson-Sivashinsky equation, which is valid for weak thermal expansion, and later by simulations carried out using a potential flow model [8]. The non-local behavior that results from the advection of wrinkles along an inclined surface was discussed by Lieuwen [9] for isothermal flows, while neglecting the influences of gas expansion. The effect on turbulent flames was studied by Lipatnikov and Chomiak [10] based on a model with spatially constant local consumption speed and growing flame brush thickness. More recently, Troiani et al. [11] and Creta et al. [12] used the local flame curvature as a key parameter for identifying the presence and impact of the DL instability on Bunsen flames. Motivated by these considerations, we examine in this paper the morphology of wrinkles created on the surface of a Bunsen flame, their advection along the flame surface and their amplification in the presence of the DL instability, as illustrated in Fig. 1. The problem is studied numerically within the context of the hydrodynamic theory and, unlike previous studies, allows for *local and temporal variations* in flame speed and

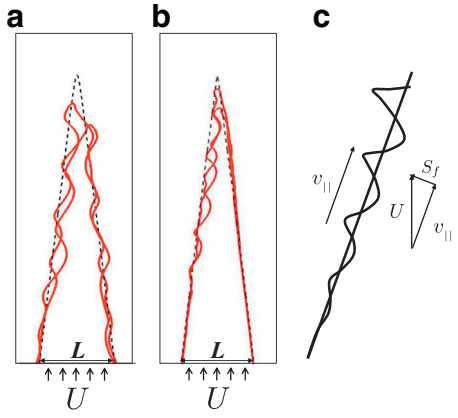


Fig. 1. Evolution of wrinkles along the surface of a Bunsen flame resulting from a numerical simulation with (a) the entire flow perturbed, and (b) only the flow on the left half of the burner perturbed. The right figure (c) is a schematic illustrating the advection and amplification of perturbations along the inclined flame surface.

examines the *nonlinear development* of perturbations under *realistic thermal expansion* conditions.

## 2. Hydrodynamic model

The hydrodynamic theory is based on the assumption that the flame thickness $l_f$ consisting of the preheat and reaction zones is much smaller than the hydrodynamic length scale $L$, represented here by the width of the burner [4,5]. In the limit $l_f/L \to 0$ the flame is confined to a surface described by $\psi(\mathbf{x}, t) = 0$ that separates the cold unburned mixture from the hot combustion products. The flow field on either side of the flame is governed by the incompressible Navier–Stokes equations with densities $\rho_u$ and $\rho_b$ for unburned and burned gas, respectively. Conservation of mass and momentum across the flame is enforced through the Rankine–Hugoniot jump relations. The instantaneous shape and location of the flame surface is described by the evolution equation

$$\psi_t + \mathbf{v}^* \cdot \nabla\psi - S_f|\nabla\psi| = 0 \tag{4}$$

where $\mathbf{v}^*$ is the gas velocity just ahead of the flame with $S_f$ given by (1). The mathematical formulation thus consists of a *nonlinear, free-boundary* problem, with all diffusion processes occurring inside the flame zone mimicked by the Markstein length $\mathcal{L}$. The flame is affected by the flow through variations in the local flame speed and the flow, in return, affected by the gas expansion resulting from the heat generated at the flame. When the problem is recast in a non-dimensional form using $L$, $S_L$, $L/S_L$ and $\rho_u S_L^2$ as units of length, velocity, time and pressure, respectively, it depends on three parameters only: thermal expansion $\sigma \equiv \rho_u/\rho_b$, the Markstein number $\mathcal{M} = \mathcal{L}/L$ and the Reynolds number.

The numerical implementation of the model is based on the hybrid Navier–Stokes/interface-tracking algorithm discussed in [13,14]. The simulations are carried out on a two-dimensional domain of width $3L$ and length $8L$, for $\mathcal{L} > 0$ corresponding to lean hydrocarbon-air or rich hydrogen-air mixtures. The two-dimensional flame surface may be viewed as the projection of an axisymmetric Bunsen flame into any cross-sectional plane. In order to clearly delineate the advection of wrinkles on the flame surface the flow has been perturbed only in the left half of the burner, retaining its nearly symmetrical but laminar shape in the other half as shown in Fig. 1(b). Perturbations are created on the flame front using a pre-generated isotropic, homogeneous turbulent flow of weak turbulence intensity $v'$, introduced at the inflow of the burner and swept into the domain with a mean velocity $U = 8S_L$. To reduce the interference of the shear flow generated near the burner edge, a weak co-flow has been introduced along the remainder of the bottom boundary. Outflow boundary conditions are imposed on all other boundaries. The density discontinuity across the flame front has been smeared over few grid points using a continuous profile [14] and the simulations carried out on a grid resolution of 64 points per unit length, sufficient to resolve the Gibson scale which, as discussed in [6], is the most relevant scale of interest here. Tests at a resolution of 128 points/length have shown variations in flame properties of at most 5–6%. Finally, we chose $\sigma = 5$, a sufficiently large Reynolds number to properly emulate the hydrodynamic model, and, unless otherwise specified, $v'/S_L = 0.1$ with an integral scale at $\ell/L = 0.1$.

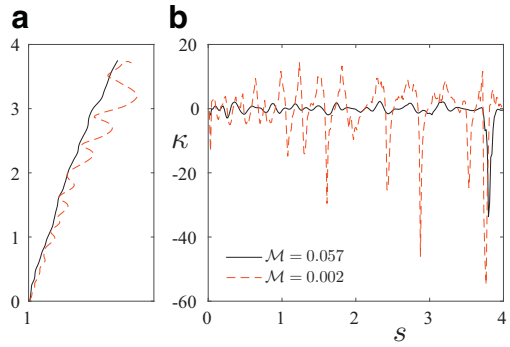


Fig. 2. (a) Snapshots of instantaneous flame profiles and (b) flame front curvature along the flame surface coordinate $s$, for $\mathcal{M} = 0.057$ (solid/black curve) and $\mathcal{M} = 0.002$ (dashed/red curve) flames.

## 3. Darrieus–Landau instability

For low turbulence intensity, Creta and Matalon [14] have identified two distinct regimes of flame propagation termed *sub-* and *super-critical* and inspired from the linear stability of a planar flame. Accordingly, $\mathcal{M} > \mathcal{M}_c$ reflected the sub-critical regime where the turbulent flame remains planar on the average, and $\mathcal{M} < \mathcal{M}_c$ the super-critical regime where the turbulent flame frequently acquires cusp-like conformations with large negative curvature, the hallmark of the DL instability [15]. The critical Markstein number for a turbulent flame must be determined numerically but can be approximated by the linear stability result of a planar flame as

$$\mathcal{M}_c = \frac{\sigma - 1}{2\pi(3\sigma - 1)}\,. \tag{5}$$

This classification is used to explain the dramatic morphological dichotomy observed in Fig. 2(a), where snapshots of instantaneous flame profiles are shown for different values of $\mathcal{M}$. The stability of inclined flames has not been discussed thoroughly in the literature; but it is evident based on the velocity decomposition shown in Fig. 1(c) that the tangential velocity component $v_\parallel$ does not affect the

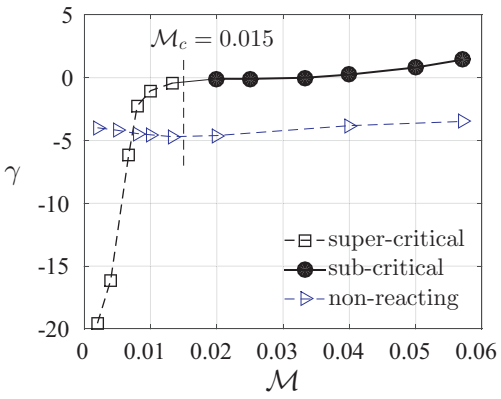


Fig. 3. Skewness of the flame front $\gamma$ curvature plotted as a function of the Markstein number, with $\mathcal{M}_c$ marking the critical value distinguishing between sub- and super-critical flames. Also plotted is the skewness of the curvature of a non-reacting surface evolving in a constant density flow due to Huygen's propagation.

growth rate of wrinkles and its role is solely to advect perturbations along the flame surface towards the tip. Thus, depending on the value of $\mathcal{M}$, flame wrinkles generated by flow perturbations are either dampened or magnified while being convected downstream. The wrinkles subside along the flame front for $\mathcal{M} = 0.057$, but increase in amplitude for $\mathcal{M} = 0.002$ with highly negative curvatures appearing downstream. The variations of local flame front curvature is plotted in Fig. 2(b) as a function of the flame surface coordinate $s$. As expected, for super-critical conditions, sharp bursts of negative curvatures are observed, indicative of the cusp-like structures and reminiscent of the DL instability. The large negative curvature near $s \approx 4$ is due to the sharp flame tip, observed for both values of $\mathcal{M}$. The presence of DL instability can be ascertained by examining the skewness $\gamma$ of the flame front curvature [11,12], which measures the extent of asymmetry from the mean in the corresponding *pdf*. For sub-critical conditions, fluctuations observed on the flame surface are solely due to turbulence. The flame exhibits moderate curvatures, both convexly and concavely, and the curvature *pdf* displays a symmetric profile with zero mean such that $\gamma \approx 0$. In contrast, perturbations of the flame surface for super-critical conditions are amplified by the DL instability. The resulting wrinkled flame exhibits localized bursts of large negative and moderate positive curvatures, and the curvature *pdf* profile is asymmetric about the mean with $\gamma$ large and negative.

This observation is used to distinguish between sub- from super-critical conditions and numerically estimate the critical Markstein number $\mathcal{M}_c$. Shown in Fig. 3 is the variation of $\gamma$ with increasing values of the Markstein number $\mathcal{M}$. The results are based only on the slanted section of the flame, avoiding the large negative curvature of the flame tip which are not associated with the DL instability. The sharp contrast in skewness, with large negative values for $\mathcal{M} < 0.015$, indicative of the presence of the DL instability, and near-zero insensitive values for $\mathcal{M} > 0.015$, suggests that $\mathcal{M}_c \approx 0.015$ for the selected $\sigma = 5$. With this value, $\mathcal{M} = 0.002$ corresponds to super-critical and $\mathcal{M} = 0.057$ to sub-critical conditions, consistent with the structures seen in Fig. 2(a). Finally, we note that the skewness $\gamma$ has been used successfully in recent DNS of Bunsen flames to identify the presence of the DL instability [11,12]. Corrugated fronts in isothermal flows also lead to the formation of cusps, or highly negative curvatures, due to Huygen's propagation; but the skewness of curvature in this case remains insensitive to variation in $\mathcal{M}$, as shown in Fig. 3. Moreover, the remarkable difference in the order of magnitude in $\gamma$ between a passive surface evolving in a constant density flow and a super-critical flame subjected to the DL instability, supports the notion that skewness is an apt parameter for identifying the onset of the hydrodynamic instability.

## 4. Advection of wrinkles

The role of DL instability in the decay/growth of wrinkles along the flame surface is examined in Fig. 4. The evolution of wrinkles is shown for the values : $\mathcal{M} = 0.057$ (sub-critical) and $\mathcal{M} = 0.002$ (super-critical), at six consecutive time intervals $\Delta t \approx 0.02$. Recall that turbulence is only introduced in the left half of the burner such that the right half retains its approximate laminar shape. For sub-critical conditions the fluctuations are dampened while being convected along the flame surface towards the flame tip, as shown in Fig. 4(a). For super-critical conditions the fluctuations are amplified along the flame surface due to the DL instability with distinctive cusp-like formations, as seen in Fig. 4(b).

The evolution of wrinkles along the flame surface is further highlighted in Fig. 5 where the instantaneous curvature along the flame coordinate $s$ is plotted for the same profiles presented in Fig. 4. Solid/open symbols are used to mark positive/negative curvatures in Fig. 5(a); only negative curvatures are shown in Fig. 5(b). Note that the ordinate in both graphs differ significantly; for $\mathcal{M} = 0.057$ the variations correspond to $|\kappa| < 10$, whereas for $\mathcal{M} = 0.002$ they correspond to $|\kappa| < 50$. For sub-critical conditions, perturbations of the flame surface are dampened and, in the absence of a preferred orientation towards the burned or unburned gas, the flame exhibits approximately equal negative and positive curvatures. Super-critical flames, on the other hand, are dominated by conformations of large negative curvatures due to the highly

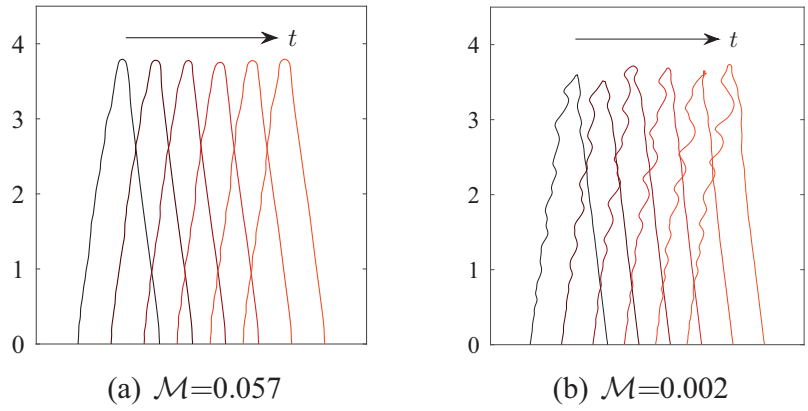


Fig. 4. Perturbed flame profiles at six consecutive times for sub-/super-critical flames; the flame is perturbed only in the left half of the burner.

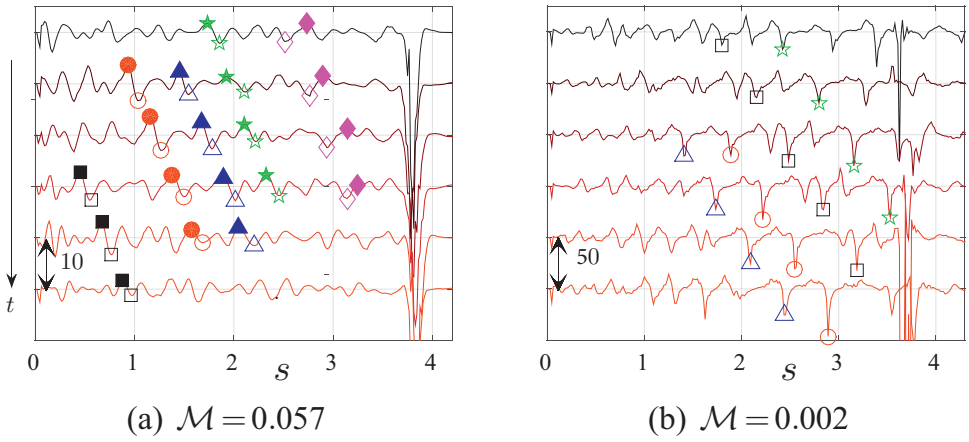


Fig. 5. Instantaneous variations in flame curvature along the coordinates $s$, for the same consecutive time intervals used in plotting the flame profiles in Fig. 4. Open symbols are used for indicating sharp crests with negative curvature and solid symbols for crests with positive curvature (used primarily for the sub-critical case). Note that the scale of the ordinate in (b) is five times larger than that in (a).

corrugated crests pointing towards the burned gas, marked by open symbols in Fig. 5(b). In both cases, the sharp negative curvatures for $s \approx 4$ must be disregarded, being the result of the highly rounded tip of the Bunsen flame. We note that the instantaneous illustration in Fig. 5 would be typically observed in an experiment. Of interest, however, is to trace back the development of perturbations to their inception time, which is discussed next.

It has been established analytically for weak thermal expansion [16], and numerically for realistic values of thermal expansion [15,17], that the flame as a result of the DL instability evolves in time to a *stable* single peak formation. In other words, the growing wrinkles due to the DL instability saturate in time to a stable constant amplitude structure. For sub-critical conditions the wrinkles on the flame surface are dampened and their amplitudes eventually tend to zero. Since the wrinkles advected on the slanted surface of a Bunsen flame survive a finite length of time before getting annihilated at the flame tip, they may not get completely dampened, or reach full saturation. A comparison of the evolution of wrinkles from the time of inception and the variation of the magnitude of their local curvature in time could then be used to quantify the impact of the DL instability. This is shown in Fig. 6 for sub- and super-critical conditions. The symbols display the values of $\kappa$ at consecutive time intervals, as in Fig. 5. For $\mathcal{M} = 0.057$ one observes a slight reduction in the magnitude of the curvature due to kinematic restoration. In contrast, for $\mathcal{M} = 0.002$ there is a clear amplification of the wrinkles advected downstream along the flame front, in ac-

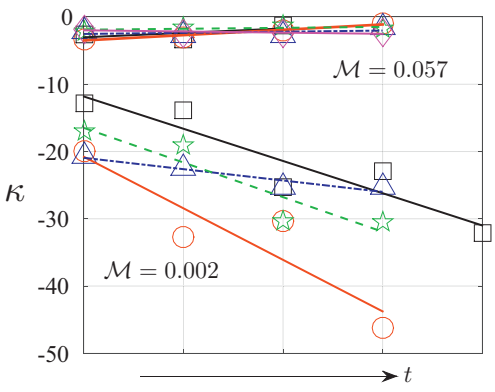


Fig. 6. Variation of the local curvature of wrinkles from inception time for sub- and super-critical conditions. Since for subcritical flames wrinkles are, on the average, equally convex as they are concave, only negative curvature values are shown.

cord with the observation in Fig. 3 that shows a large negative skewness. The noise in the data is primarily due to the background fluctuations of the velocity field which continuously perturb the flame front, but owing to the weak turbulence intensity the resulting perturbations are small relative to the dominant DL instability effects. The extent to which wrinkles at a given location along the flame correlate to upstream perturbations can be assessed using the spatial-temporal correlation function

$$R(s,t\,;\xi_s,\tau) = \frac{\overline{\kappa(s+\xi_s,t-\tau)\,\kappa(s,t)}}{\sqrt{\overline{\kappa(s+\xi_s,t-\tau)^2}}\,\sqrt{\overline{\kappa(s,t)^2}}}$$

where the local curvature $\kappa$ has been used to characterize a wrinkle (here the "overbar" stands for the time-averaged mean). Accordingly, $R$ represents the correlation of a wrinkle at position $s$ and time $t$ to an incoming fluctuation at $s+\xi_s$ and time $t-\tau$. Choosing $s = 2.8$ as a reference position located close to the flame tip, the variations of $R$ with neighboring locations ($\xi_s < 0$) up to the burner rim, are shown in Fig. 7(a) for various times $\tau$. The colored/marked curves are plotted for $\mathcal{M} = 0.002$ (super-critical) with the various colors/symbols representing different times $\tau$. As expected, when $\tau = 0$, the correlation function $R$ has a maximum at the reference position $s = 2.8$ (or $\xi_s = 0$) and spreads over a short distance before dropping to beneath $R = 0.2$, below which the wrinkles may be considered uncorrelated. Subsequent curves of $R$ have similar shapes, but with peaks of decreasing magnitude that are shifted upstream when $\tau$ increases. The spatial extent of these curves, shown by the black solid curve in the figure, represents the distance over which wrinkles are correlated over time. These results may be understood if disturbances on the flame surface are viewed to consist of a "local component" due to turbulent fluctuations and a "non-local" component resulting from wrinkles amplified by DL effects and convected from an upstream location along the flame. The preceding picture may be contrasted to the correlation of wrinkles on the surface of a planar flame, shown in Fig. 7(b) for the same value of $\mathcal{M} = 0.002$. The mean flow velocity is now normal to the flame surface and the wrinkles, which are always centered around the reference location, here selected arbitrarily at $s = 0.8$, become uncorrelated over time. For $\mathcal{M} = 0.057$, the correlation function exhibits a similar but weaker dependence on upstream conditions and over a shorter distance

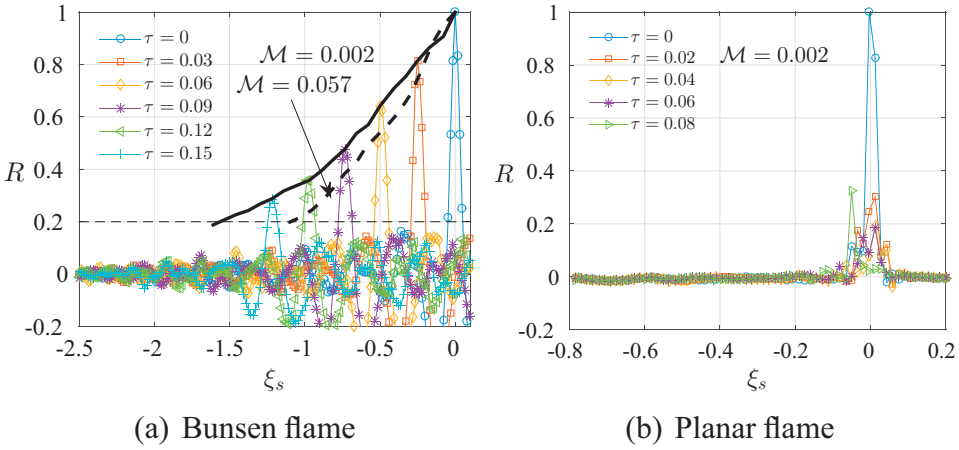


(a) Bunsen flame (b) Planar flame

Fig. 7. Correlation of the local flame curvature along the flame surface at different times $\tau$ with respect to a reference position near the flame tip; for $\mathcal{M} = 0.002$. The dashed curve in (a) represents the peak values of $R$ for $\mathcal{M} = 0.057$ (the actual data is not shown).

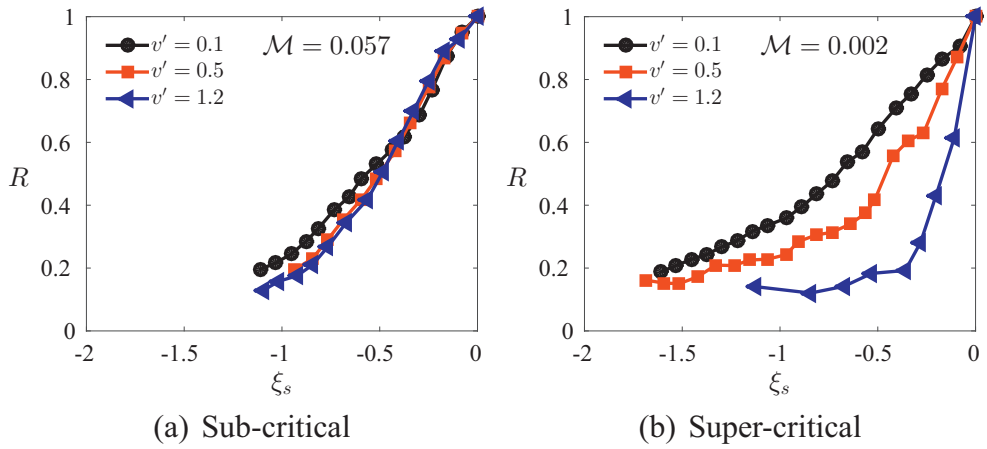


Fig. 8. Peaks of correlation functions $R$ vs the distance (upstream) from the flame tip, for different turbulence intensities.

as shown by the dashed black curve in the figure. The planar flame in this case will be stable such that fluctuations of the flame surface are solely due to turbulence, and $R \approx 0$ in this case.

The sensitivity of the correlation function $R$ to turbulence intensity $v'$ is shown in Fig. 8, where the peaks of the correlation functions are plotted as a function of $\xi_s$, for sub- and super-critical conditions. When increasing $v'$ for super-critical conditions, the local contribution to wrinkling caused by the fluctuating turbulent field becomes more notable and eventually comparable to the amplification due to the DL instability. This leads to a weaker "memory" effect, causing a sharp drop in the correlation function. In contrast, for sub-critical conditions the wrinkles are predominantly due to the turbulent fluctuations and the correlation function remains insensitive to variations in turbulence intensity.

## 5. Distribution of interfacial properties

In Fig. 9, the non-local contribution to wrinkling for Bunsen flames is contrasted to (i) a planar flame in a turbulent flow, and (ii) a passive Bunsen-like interface in a non-reacting (constant-density) turbulent flow, of equal intensities. The figure shows the variations of the local curvature of the flame surface, or interface, along the surface for each of the three cases, and for both $\mathcal{M} = 0.002$ and $\mathcal{M} = 0.057$. The extent of the distribution represents the thickness of the flame brush.

When comparing the distribution of $\kappa$ for the Bunsen flame and the passive interface, two significant differences are observed, both associated with thermal expansion. First, the passive interface appears insensitive to variations in Markstein number and has an almost flat distribution along its surface up to the highly rounded tip, whereas the Bunsen

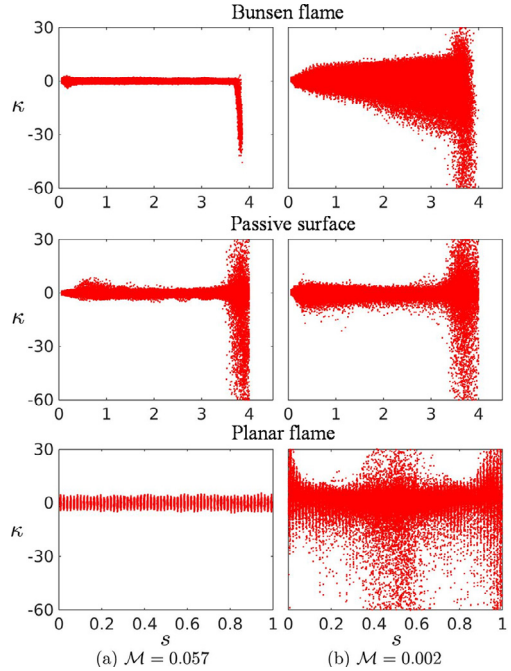


Fig. 9. Distribution of $\kappa$ along the flame coordinate $s$ for a Bunsen flame, a passive Bunsen-like surface and a planar flame.

flame exhibits a marked difference with the curvature distribution widening downstream for super-critical conditions ($\mathcal{M} = 0.002$) due to amplification of wrinkles by the DL instability. Second, for sub-critical conditions the Bunsen flame displays a much narrower curvature distribution compared to the passive interface, which results from the stabilization influences of diffusion absent in the latter. The distribution of curvature along the

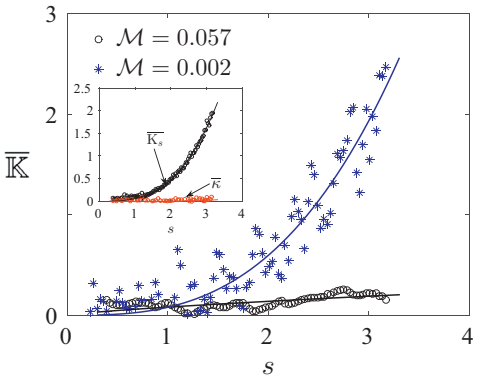


Fig. 10. Variations of mean local flame stretch along the flame surface for sub- and super-critical conditions; the individual contributions of curvature and strain for $\mathcal{M} = 0.002$ are shown in the inset.

surface of a planar flame is significantly different for sub- and super-critical flames, but in both cases it is spread randomly along the surface due to the absence of an advection velocity component. For $\mathcal{M} = 0.057$ the flame brush is thin and nearly-planar; whereas for $\mathcal{M} = 0.002$ the flame is much thicker and exhibits highly negative curvatures [6]. The difference between the curvature distribution along the surface of a Bunsen and a planar flame occurs primarily under super-critical conditions and is evidently due to their distinct geometric configurations. The distribution of $\kappa$ along the surface of a Bunsen flame exhibits an upstream influence, whereby wrinkles with large curvatures due to the DL instability are advected downstream and thus concentrated closer to the flame tip, resulting in a thicker flame brush; unlike the passive interface which retains a nearly constant thickness. These observations indicate that the "memory" effect in Bunsen flames results from the underlying flow field associated with its geometric configuration combined with thermal expansion, and the absence of either is insufficient to create the "non-local" dependence on upstream conditions along the flame. For example, the passive interface, despite having a tangential velocity component along its surface shows no dependence on upstream conditions due to the absence of thermal expansion. Similarly, the planar flame with an active thermal expansion lacks any such preferred correlation due to its flat shape.

Although the aforementioned "memory" effect critically modifies the appearance and local properties of turbulent flames, variations in *inherent* flame properties properly account for this effect. For example, the mean local stretch rate $\overline{\mathbb{K}} = S_L\overline{\kappa} + \overline{K}_s$ consisting of the effects of curvature $\kappa$ and hydrodynamic strain $K_s$, is contained in the determination of the turbulent flame speed $S_T$. Plotted in Fig. 10 is the variation of $\overline{\mathbb{K}}$ along a Bunsen flame surface, with the individual contributions of curvature and strain shown in the inset for the super-critical case (excluding the large curvature near the flame tip). Under turbulent conditions the flame is weakly stretched by velocity fluctuations and, since wrinkles created near the burner rim are advected along the surface, the mean stretch rate $\overline{\mathbb{K}}$ is expected to increase with increasing $s$. For sub-critical conditions, only a small increase in $\overline{\mathbb{K}}$ is observed because, the wrinkles created on the flame surface and advected downstream are dampened by the stabilizing influences of diffusion. For super-critical conditions, $\overline{\mathbb{K}}$ increases substantially with $s$ due to the amplification of wrinkles advected along the flame front. The figure also clearly shows that hydrodynamic strain is the primary contributor to stretch, as reported in [6].

## 6. Conclusions

The Bunsen flame is widely used to investigate the behavior of premixed flames under turbulent conditions in the laboratory due to the simplicity of establishing and controlling the flame. The incoming flow has a velocity component tangential to the inclined surface, which is integral in the advection of wrinkles created on the flame front towards the flame tip. Disturbances on the flame surface may thus be viewed as consisting of a local contribution resulting from velocity fluctuations and a non-local contribution resulting from wrinkles created near the burner rim and advected downstream. For weak turbulence intensities the morphology of the flame surface depends strongly on whether or not local disturbances are amplified by the DL instability, conditions referred to as super- and sub-critical, respectively. The highly wrinkled flames, which are a consequence of the DL instability exhibit frequent bursts of negative curvatures resulting in an asymmetric curvature *pdf*; quite distinct from the symmetric *pdf* observed in the absence of the instability. The skewness of curvature, therefore, is a suitable marker for determining the critical conditions, expressed in terms of a Markstein number $\mathcal{M}_c$. The morphology of the flame changes dramatically when $\mathcal{M}$ is above/below $\mathcal{M}_c$. For sub-critical conditions, with $\mathcal{M} > \mathcal{M}_c$, the wrinkles created near the burner rim subside when advected along the weakly perturbed flame front and the relatively thin flame brush remains nearly constant. For super-critical conditions with $\mathcal{M} < \mathcal{M}_c$, the wrinkles are amplified when advected along the flame front leading to a flame brush that becomes thicker further downstream. A measure of these noteworthy changes in flame behavior manifests itself in the mean local stretch rate, which is modulated by $\mathcal{M}$ and has a direct effect on the turbulent flame speed.

## Acknowledgments

Meng Zhang acknowledges the National Natural Science Foundation of China (51706172) and Post Doctoral Foundation of China (2017M613130) for the financial support and Xian Jiaotong University for the computational resources.

## References

[1] G. Searby, J.-M. Truffaut, G. Joulin, *Phys. Fluids* 13 (11) (2001) 3270–3276, doi:10.1063/1.1407815.
[2] J. Driscoll, *Prog. Energy Combust. Sci.* 34 (1) (2008) 91–134, doi:10.1016/j.pecs.2007.04.002.
[3] G. Damköhler, *Z. Elektrochem.* 46 (1940) 601–652.
[4] M. Matalon, B.J. Matkowsky, *J. Fluid Mech.* 124 (-1) (1982) 239, doi:10.1017/S0022112082002481.
[5] M. Matalon, C. Cui, J.K. Bechtold, *J. Fluid Mech.* 487 (2003) 179–210, doi:10.1017/S0022112003004683.
[6] N. Fogla, F. Creta, M. Matalon, *Combust. Flame* 162 (7) (2015) 2758–2777, doi:10.1016/j.combustflame.2015.04.012.
[7] L. Boyer, J. Quinard, *Combust. Flame* 82 (1990) 51–56.
[8] B. Denet, *Phys. Fluids* 14 (2002) 3577–3583.
[9] T. Lieuwen, *Unsteady Combustor Physics*, Cambridge University Press, 2012.
[10] A. Lipatnikov, J. Chomiak, *Prog. Energy Combust. Sci.* 28 (1) (2002) 1–74, doi:10.1016/S0360-1285(01)00007-7.
[11] G. Troiani, F. Creta, M. Matalon, *Proc. Combust. Inst.* 35 (2) (2015) 1451–1459, doi:10.1016/j.proci.2014.07.060.
[12] F. Creta, R. Lamioni, P.E. Lapenna, G. Troiani, *Phys. Rev. E* 94 (2016) 053102, doi:10.1103/PhysRevE.94.053102.
[13] Y. Rastigejev, M. Matalon, *Combust. Theory Model.* 10 (3) (2006) 459–481, doi:10.1080/13647830500463502.
[14] F. Creta, M. Matalon, *J. Fluid Mech.* 680 (2011a) 225–264, doi:10.1017/jfm.2011.157.
[15] F. Creta, M. Matalon, *Proc. Combust. Inst.* 33 (1) (2011b) 1087–1094, doi:10.1016/j.proci.2010.06.029.
[16] D. Vaynblat, M. Matalon, *SIAM J. Appl. Math.* 60 (2) (2000) 679–702, doi:10.1137/S0036139998346439.
[17] Y. Rastigejev, M. Matalon, *J. Fluid Mech.* 554 (-1) (2006) 371, doi:10.1017/S0022112005008098.